NJC

ROYAL SOCIETY OF CHEMISTRY

PAPER

View Article Online
View Journal | View Issue

Cite this: *New J. Chem.*, 2023, **47**, 10751

Magnetic graphene noble metal aerogels: preparation and application for catalytic degradation of 4-NP

Danyi Li,[ab] Lin Lin,[ab] Manli Lu,[ab] Linfan Li [ab] and Jihao Li *[ab]

Received 4th March 2023,
Accepted 1st May 2023

DOI: 10.1039/d3nj01041d

rsc.li/njc

In this work, the preparation of magnetic graphene noble metal aerogels (GA–Fe_3O_4–$Au_{-ethanol}$) was realized by self-assembly induced by radiation reduction. The prepared material GA–Fe_3O_4–$Au_{-ethanol}$ can be easily attracted by a magnet. Meanwhile, GA–Fe_3O_4–$Au_{-ethanol}$ successfully realized the degradation of 4-nitrophenol (4-NP), which was considered an environmentally harmful pollutant. It is worth mentioning that the prepared materials showed a better catalytic performance than general noble metal catalysts, and it was found that the content of noble metals in the fabricated composite significantly influenced the catalytic reaction rate. The successful preparation of this material provides a feasible scheme for treating pollutant 4-NP.

1. Introduction

Noble metal nanoparticles are often used in medicine and environmental research because they have unique biophysical properties, mainly due to their highly accessible surface. Among a series of noble metal nanoparticles, Au nanoparticles have received the most attention from researchers.[1] Conventionally, AuNPs are synthesized using chemical substances as reducing agents.[2] Due to the chemical-reducing agents being generally toxic and easily polluting the environment, developing environmentally friendly nano-synthetic routes is of high importance. Preparing noble metal nanoparticles by radiation reduction is a greener preparation method than traditional chemical methods.[3]

Catalytic reduction of 4-nitrophenol using metal-based catalysts is an important reaction that typically employs noble metals such as palladium, rhodium, and platinum, as well as transition metals such as iron, nickel, and cobalt.[4–6] In this reaction, the catalyst acts as a reducing agent, and under catalysis, the nitro group is reduced to an amino group.

The choice of catalyst depends on factors such as reaction conditions, catalyst cost, and reaction rate. For example, palladium-based catalysts have high catalytic activity and selectivity, and are suitable for many reduction reactions, but are expensive. Therefore, some studies have attempted to use inexpensive catalysts such as nickel, iron, and others.[7,8]

This reaction has broad application prospects, for example, it can be used in the preparation of organic chemicals, pharmaceuticals, and dyes. Additionally, the reaction can also be used in areas such as wastewater treatment and air pollution control. Therefore, catalytic reduction of 4-nitrophenol using metal-based catalysts is an important research area that attracts widespread attention and study.

Nitroaromatic compounds are widely employed in manufacturing pharmaceuticals, pigments, dyes, plastics, pesticides, fungicidal agents, explosives, and industrial solvents. However, considering its industrial production and potential environmental pollution, 4-NP has been regarded as the most important of the mononitrophenols.[9] Among the metal NPs, AuNPs generated under various conditions are known to be efficient catalysts for reducing organic dyes and reducing 4-nitrophenol (4-NP) to 4-aminophenol (4-AP).[10] A lot of research studies have reported combing nanogold with some substrates to prepare nanogold materials with small size and uniform dispersion, such as combining nanogold with polymers,[11] inorganic metal materials,[12] and with graphene oxide.[13] Among them, the materials prepared by Au and graphene oxide are often tricky because they are challenging to recover.[14] In this paper, by introducing magnetic iron oxide into composites, we hope to obtain materials that can be attracted and controlled using magnets to solve the problem of difficulty in recovering materials to a certain extent.

Herein we report the synthesis of a GA–Fe_3O_4–$Au_{-ethanol}$ composite using a mild one-step method. We used reducing substances produced by irradiating water at 200 KGy in the presence of ethanol. The Au NPs produced in the reaction get attached to the graphene sheets and are stable for weeks

[a] *Shanghai Institute of Applied Physics, Chinese Academy of Sciences, Shanghai, China. E-mail: lijihao@sinap.ac.cn*
[b] *University of Chinese Academy of Sciences, Beijing 100049, China*

without a noticeable change in their properties. The AuNPs made were small, with sizes below 5 nm, and were found to show high catalytic activity. The amount of AuNPs produced could be easily controlled by controlling the starting materials ($AuCl_3{\cdot}HCl{\cdot}4H_2O$). Also, due to the addition of Fe_3O_4 NPs, the material can be easily attracted by the magnet. We have studied the catalytic reduction of 4-NP to 4-AP by the composite using $NaBH_4$ as the reducing agent under heterogeneous conditions. When the heterogeneous catalytic reaction was carried out in the presence of excess $NaBH_4$, it was observed to follow pseudo-first-order kinetics, and the apparent reaction rate constant depended linearly on the concentration of AuNPs present in the composite.

2. Experimental section

2.1 Reagents and materials

GO was synthesized from natural graphite flakes using a modified Hummers' method.[15] Fe_3O_4, ethanol, and $AuCl_3{\cdot}HCl{\cdot}4H_2O$ were obtained from Sinopharm Chemical Reagent Co., Ltd (Shanghai, China). Besides, the solvents used in the experiment are analytical grade and require no further purification.

2.2 Synthesis of GA–Fe_3O_4–$Au_{-ethanol}$ composites by γ-ray irradiation

The process of preparing GA–Fe_3O_4–$Au_{-ethanol}$ composites is shown in Fig. 1. First, 0.0136 mmol L^{-1} Fe_3O_4 was added into GO solution (2 mg mL^{-1}) and stirred thoroughly (ultrasonic stirring is recommended because Fe_3O_4 will interact with a magnetic stirrer), Then chloroauric acid solution with different concentrations (0.02 mg mL^{-1}, 0.1 mg mL^{-1}, 0.2 mg mL^{-1}, 0.4 mg mL^{-1}, and 0.8 mg mL^{-1}) was added to the above solution and stirred separately. Finally, the solvent (ethanol and water 1 : 1) was added to the above mixture and stirred for 2–3 h. Subsequently, the above-mixed solution was put into a 50 mL small bottle, about two-third of the bottle, then nitrogen was blown into the bottle (for 5–10 min) to create an inert environment in the bottle, and the bottle was covered. Finally, the above samples were irradiated at room temperature for 17 h with a dose of 200 kGy. After irradiation, graphene/Fe_3O_4/Au composite hydrogels (GH–Fe_3O_4–$Au_{-ethanol}$) were obtained, and then the obtained GH–Fe_3O_4–$_{ethanol}$ was washed 10 times with ethanol/water solution to remove ionic impurities and other organic molecules. Following that, GA–Fe_3O_4–$Au_{-ethanol}$ aerogels were obtained by freeze-drying GH–Fe_3O_4–$Au_{-ethanol}$ at −40 °C and 0.14 kPa. Through the same steps, the samples obtained with different Au contents were labeled as GA–Fe_3O_4–$Au_{-ethanol}$ 0.02 mg mL^{-1}, GA–Fe_3O_4–$Au_{-ethanol}$ 0.1 mg mL^{-1}, GA–Fe_3O_4–$Au_{-ethanol}$ 0.2 mg mL^{-1}, GA–Fe_3O_4–$Au_{-ethanol}$ 0.4 mg mL^{-1} and GA–Fe_3O_4–$Au_{-ethanol}$ 0.8 mg mL^{-1}, respectively. And the sample without chloroauric acid was also prepared as the control and labeled as GH–Fe_3O_4–$_{ethanol}$.

2.3 Catalytic degradation of 4-NP

We measured the process of the composite catalysis experiment using a UV-VIS spectrometer, and the scanning wavelength range was 200–700 nm. During continuous stirring, 10 mg GA was added as a catalyst to the 4-NP (20 mL 0.5 mmol L^{-1}) solution, and then the newly prepared $NaBH_4$ aqueous solution (10 mL 0.5 mol L^{-1}) was quickly added to the above solution. All catalytic reactions were stirred in a 50 mL small beaker at a speed of 150 rpm. Then the reaction process was monitored using UV-VIS spectroscopy. The kinetic rate constant k of the first-order reaction can be calculated using the formula (1)

$$\ln\left(\frac{C_t}{C_0}\right) = -kt \quad (1)$$

C_0 is the initial concentration of 4-NP and C_t is the concentration of 4-NP in the reaction.

2.4 Adsorption of organic solvents

A certain mass of material (m_b) was weighed and placed in dodecane for a period to achieve adsorption equilibrium. The mass of material (m_a) was weighed after adsorption of organic solution. The formula $(m_a - m_b)/m_a$ was used to calculate the adsorption capacity of the material. After that, the material

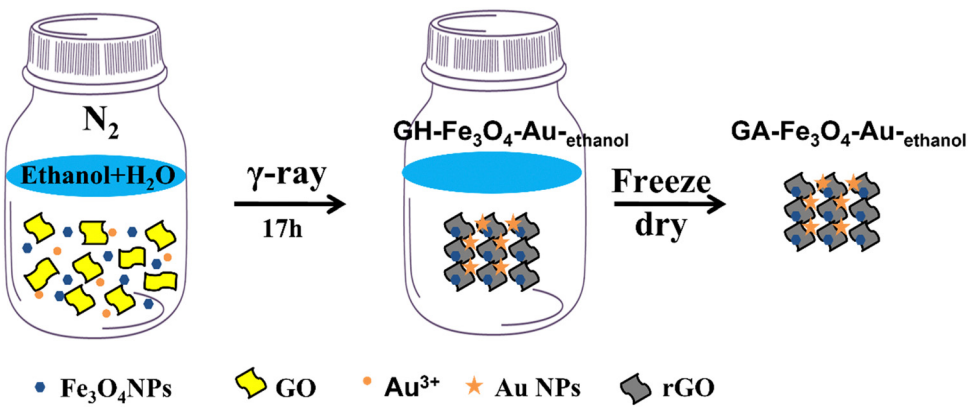

Fig. 1 Schematic illustration of the synthesis process of GA–Fe_3O_4–$Au_{-ethanol}$. In the figure, GO represents graphite oxide, GH represents graphene hydrogel, GA represents graphene aerogel, and rGO represents reduced graphite oxide.

adsorbed with the organic solution was dried. This step was repeated to test the cyclic adsorption capacity of the material.

2.5 Characterization of GA–Fe_3O_4–Au–$_{ethanol}$ composites

The microstructure of GA–Fe_3O_4–Au–$_{ethanol}$ composite aerogels was observed using a field emission scanning electron microscope (FESEM, JSM-6700F, JEOL, Ltd Tokyo, Japan) at an accelerating voltage of 5.0 kV. T. A high-resolution transmission electron microscope (HR-TEM; JEM-3000F, JEOL, Ltd) was used to observe the distribution of Fe_3O_4 NPs on graphene. The crystal structure of GA–Fe_3O_4–Au–$_{ethanol}$ composites was measured using an X-ray diffractometer (XRD, Bruker D8, Germany) with a Cu-Ka radiation source (λ =1.54 Å) at 40 kV and 50 mA.

3. Results and discussion

3.1 Morphology of GA–Fe_3O_4–Au–$_{ethanol}$ composites

It can be seen from Fig. 2a that the height of the composite is about 3.2 cm, the diameter of the bottom is about 2 cm, and the apparent morphology of the composite is similar to the appearance of the container used for preparation, which implies that the container used for preparation may directly affect the appearance of the prepared material. Therefore, it is expected that composites of any shape can be produced by controlling the shape of the container.

The composite was further analyzed using SEM. As shown in Fig. 2e, the material's interior has a porous network structure due to the mutual overlap and self-assembly of graphene oxide after reduction.[16] At the same time, tiny particles can be seen attached at the edge of the porous channel, with a diameter of about 1 μm or less. It is preliminarily considered that they are Fe_3O_4 nanoparticles added to the material. Fig. 2c shows the outer surface of the composite material. It can be seen that its outer surface is relatively flat and doped with small particles. This is because the material's outer surface is in direct contact with the wall of the container used in the preparation process, which limits the assembly between graphene oxide sheets. Here, we also preliminarily believe that the tiny particles attached to the surface are Fe_3O_4 nanoparticles. Meanwhile, using magnets can easily attract materials, as shown in Fig. 2b. This also shows the successful introduction of Fe_3O_4 on the one hand. To further characterize the morphology of the material, the material was observed using a transmission electron microscope, as shown in Fig. 2d. It was found that the diameter of Au nanoparticles was 15–30 nm, and the Au nanoparticles were found to be evenly distributed on the graphene layer. At the same time, Fe_3O_4 with a diameter of about 60 nm was also observed. (Nano Fe_3O_4 exhibits a cubic crystal structure and its particle size is consistent with that of the iron tetroxide we purchased, with a particle size of 50–100 nm.) The above results further illustrate the successful preparation of the material.

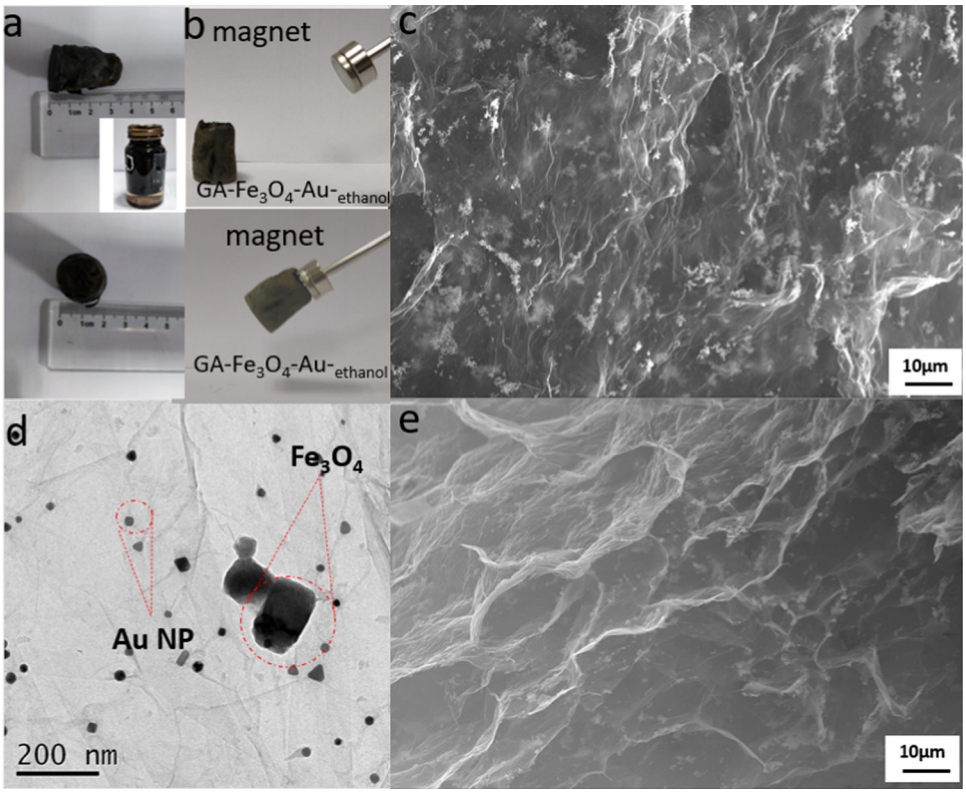

Fig. 2 (a) Appearance and dimensions of composite materials and the corresponding containers. (b) GA–Fe_3O_4–Au–$_{ethanol}$ attracted by a magnet. (c) Surface topography of GA–Fe_3O_4–Au–$_{ethanol}$. (d) TEM image of GA–Fe_3O_4–Au–$_{ethanol}$. (e) Internal morphology of GA–Fe_3O_4–Au–$_{ethanol}$.

3.2 FI-IR/XPS/XRD characterization

To determine the elemental composition of the material, X-ray photoelectron spectroscopy (XPS) measurements were carried out revealing the presence of C, Fe, O, and Au elements in GA–Fe_3O_4–Au–$_{ethanol}$ as shown in Fig. 3a. Meanwhile, Fig. 3b shows the high-resolution XPS spectrum of Au 4f measured on the GA–Fe_3O_4–Au–$_{ethanol}$ surface. The peak value of Au $4f_{7/2}$ is 83.8 eV, indicating that gold does exist in the form of uncombined atoms.[17] The above conclusion shows that the reduction of Au^{3+} can be achieved through radiation reduction, and the prepared composites contain Au^0.

As shown in Fig. 3c, the bands at 1632 cm^{-1} in the GA–Fe_3O_4–Au–$_{ethanol}$ spectrum are attributed to the stretching vibrations of C=O in the quinone-like structure.[18] Compared with the original GO spectrum, the intensity of the peak at about 1632 cm^{-1} is reduced, indicating that graphene oxide has been reduced. The characteristic vibration peaks of GO are the broad and intense peak of O–H groups centered at 3400 cm^{-1}, the strong C=O peak at about 1735 cm^{-1}, the O–H deformation peak at about 1400 cm^{-1}, the C–OH stretching peak at about 1256 cm^{-1}, and the C–O stretching peak at about 1080 cm^{-1}.[19] The reduction of graphene oxide can also be explained by the reduction of the carboxyl peak located at about 1735 cm^{-1}.

The XRD spectra of GA–Fe_3O_4–Au–$_{ethanol}$ are shown in Fig. 3d, and are compared with the XRD spectrum of graphene oxide. It can be found that the characteristic peaks belonging to GO disappear at about 12°, and a broad peak belonging to graphite appears at about 23° due to the removal of oxygen-containing functional groups. The peak at 23° is assigned to the (002) crystal plane of graphite, confirming the formation of rGO sheets. And the broad rise of the peak was caused by the disordered stack of rGO sheets and structural defects.[20] Compared with the XRD spectrum of GA–Fe_3O_4–ethanol, the X-ray diffraction patterns of both composites show five sharp peaks at approximately 30.43°, 35.75°, 43.36°, 57.29° and 62.87°, which represent different crystal planes of Fe_3O_4, suggesting the successful incorporation of Fe_3O_4 nanoparticles. At the same time, compared with GA–Fe_3O_4–ethanol composites, it is found that there are distinctive diffraction peaks at 2θ = 38.5°, which belong to the (1 1 1) planes of the cubic phase of Au.[21] It shows that radiation reduction successfully introduces Au nanoparticles into the composites.

3.3 Vibrating sample magnetometry (VSM) characterization

The magnetic properties of the GA–Fe_3O_4–Au–$_{ethanol}$ composite were studied using VSM. Fig. 4 shows the hysteresis loop of the composite obtained by applying an external field between −2 and 2 T at room temperature. The magnetization curve reveals that the composite exhibits superparamagnetic properties at room temperature, without remanence or coercivity.[22] Superparamagnetism refers to the characteristic of being responsive

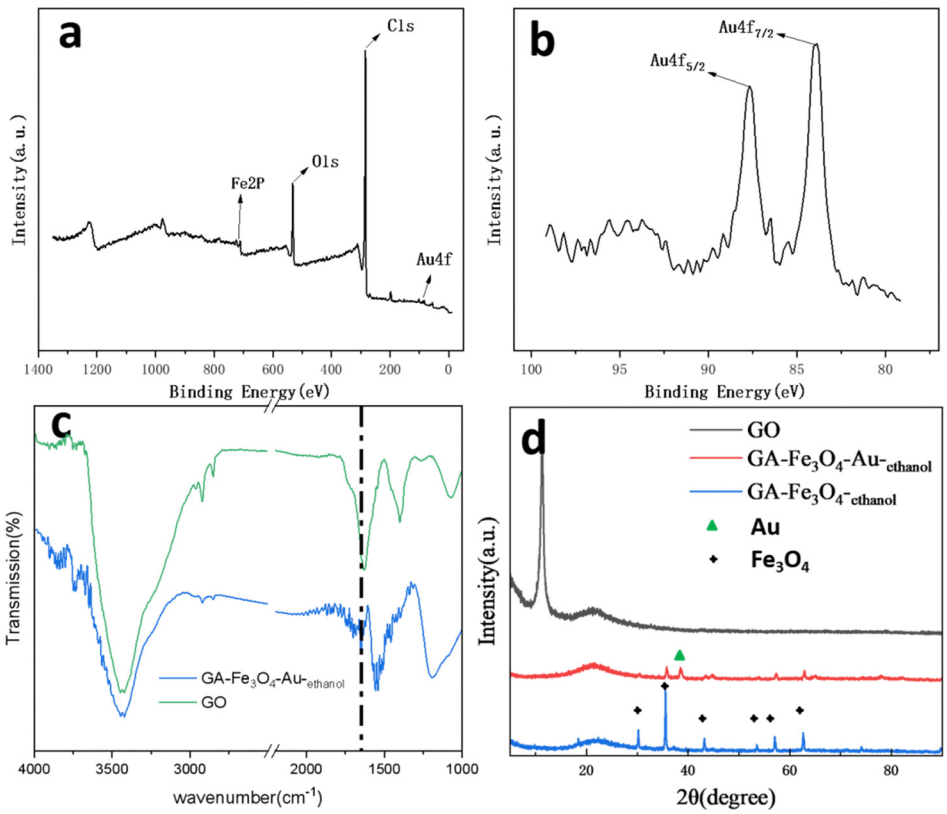

Fig. 3 (a) XPS survey spectrum of GA–Fe_3O_4–Au–$_{ethanol}$ (b) the Au 4f high resolution XPS spectrum of GA–Fe_3O_4–Au–$_{ethanol}$. (c) FT-IR spectra of GA and GA–Fe_3O_4–Au–$_{ethanol}$. (d) XRD spectra of GA–Fe_3O_4–Au–$_{ethanol}$, GA–Fe_3O_4–$_{ethanol}$, and GO.

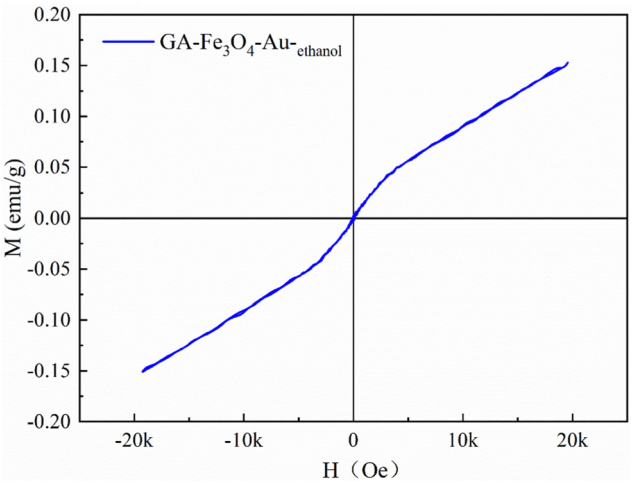

Fig. 4 *M–H* curve of the GA–Fe_3O_4–$Au_{-ethanol}$ composite at room temperature.

to an applied magnetic field but not retaining any magnetism after removal of the field. The composite's superparamagnetic properties can prevent the formation of aggregates caused by residual magnetism after the external field is removed.

3.4 Analysis of catalytic reduction of 4-NP

Using c = 0.5 mol mL^{-1} $NaBH_4$ as a reducing agent, 4-NP with a concentration of c = 0.5 mmol mL^{-1} was catalytically reduced. The process diagram of the catalytic reaction is shown in Fig. 5a. The solution becomes transparent as the reaction proceeds. As a model reaction, the catalytic reaction was easy to study using the UV-VIS spectrum as shown in Fig. 5b–d. The absorption peaks at 400 and 300 nm correspond to 4-NP and 4-AP(Fig. 5b), respectively. In the UV-VIS Spectrum, the decrease of the absorption peak at 400 nm and the increase of the absorption peak at 300 nm indicate that 4-AP is generated. That is, the catalytic reaction is in progress. The disappearance of the characteristic peak at 400 nm represents the full completion of the catalytic reaction. The catalytic efficiency is further improved by the increased loading of AuNPs in GA materials. The corresponding $\ln(C_t/C_0)$ *versus* the time curve at 400 nm is shown in Fig. 5d, and shows that the kinetic reaction constants are 0.12 min^{-1}, 0.12 min^{-1}, and 0.25 min^{-1}, respectively. Compared with other literature reports, such as Xiong, LL, *etc.*, our work only uses 0.02 mM metal nanoparticles to achieve a similar catalytic effect.[23] Compared to what Zhang, RF *et al.* reported, our work achieved faster degradation of 4-NP, completing the catalytic degradation of 4-NP in less than 20 minutes.[24] It can be seen that GA–Fe_3O_4–$Au_{-ethanol}$ shows excellent performance for the catalytic reduction of 4-NP, following pseudo-first-order kinetics and, what is more, the apparent rate constant depended linearly on the concentration of Au NPs present in the composite.

3.5 Organic dye adsorption

As the graphene sheet has the potential ability to adsorb organic dye solution, we tested the ability of the composite to adsorb organic dye solution. As shown in Fig. 6b, a certain quantity of the composite was added to a specific concentration of methylene blue solution and kept for a while until the adsorption reaches equilibrium (it takes 12 h to reach adsorption equilibrium). UV-VIS spectrometry was used to characterize a particular volume of the adsorbed dye solution. It was found that the composite has a specific ability to adsorb methylene blue. We also carried out the same experiment on the adsorption of rhodamine using the composite, as shown in Fig. 6c. The results show that the composite also has a particular ability to adsorb rhodamine. The change before and after the adsorption of organic dye solution is not evident through direct observation with the naked eye, which may be caused by too few composite materials and too high a concentration of the organic dye solution.

At the same time, the adsorption capacity of the material for 4-NP was also tested, as shown in Fig. 6a. It was found that the material had a specific adsorption capacity to 4-NP, and the material reached adsorption equilibrium in 3 h. This result shows that the material can adsorb a certain amount of 4-NP in the experiment of catalytic degradation of 4-NP. Still, the amount of adsorption must be increased to make the reaction system clear and transparent. The clarification of the solution after the reaction is due to the occurrence of a substantial catalytic response rather than simple adsorption. The adsorption of 4-NP on the materials is also conducive to the enrichment of 4-NP, which makes the catalytic reaction rate faster.

3.6 Adsorption of organic solution

The adsorption evaporation curve of the material for cyclic adsorption of *n*-dodecane is shown in Fig. 7. It can be seen that the material can adsorb *n*-dodecane with a maximum mass of about 50 times its own and maintain good adsorption stability in recycling adsorption. Compared to the GA–Fe_3O_4–$Au_{-ethanol}$ materials prepared previously,[25] it was found that the introduction of AuNPs did not adversely affect the adsorption capacity of the materials.

3.7 BET analysis

By employing BET analysis, we have analyzed the pore structure of the material, and the test results, as depicted in Fig. 8, reveal that the material possesses a fairly large specific surface area of about 78.79 $m^2\ g^{-1}$, with an average pore size of 12.58 nm. This is advantageous for the application of the material in the field of catalysis, as the high specific surface area offers more abundant catalytic binding sites. From the desorption isotherm, it can be inferred that initially, adsorbed molecules tend to aggregate around the most attractive sites on the surface. As the adsorption progresses, a self-accelerating phenomenon emerges. The observed type III adsorption isotherm suggests that the material at hand is macroporous. The adsorption–desorption isotherm curve for nitrogen displays a H3 hysteresis loop, without any conspicuous saturated adsorption platform, indicating an irregular pore structure. The H3-type hysteresis loop stems from flake-particle materials and cracked pore materials, which can be deemed as slit pores formed by

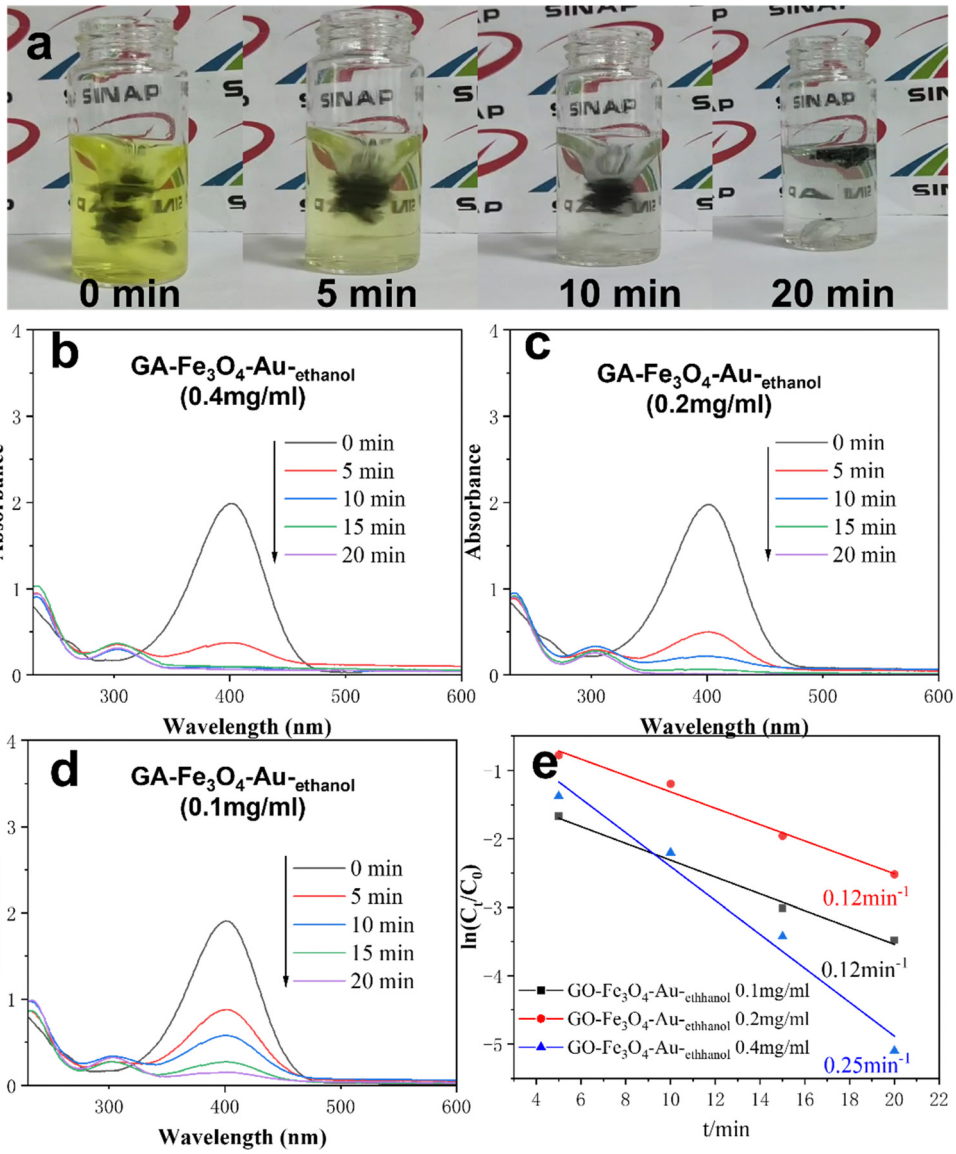

Fig. 5 (a) The color of the solution changes with the progress of the catalytic reaction (0.4 mg mL^{-1} GA–Fe_3O_4–Au–$_{ethanol}$ was used).(b–d) UV-VIS spectrum of GA–Fe_3O_4–Au–$_{ethanol}$ for catalytic degradation of 4-NP. (e) The corresponding $\ln(C_t/C_0)$ *versus* time curve.

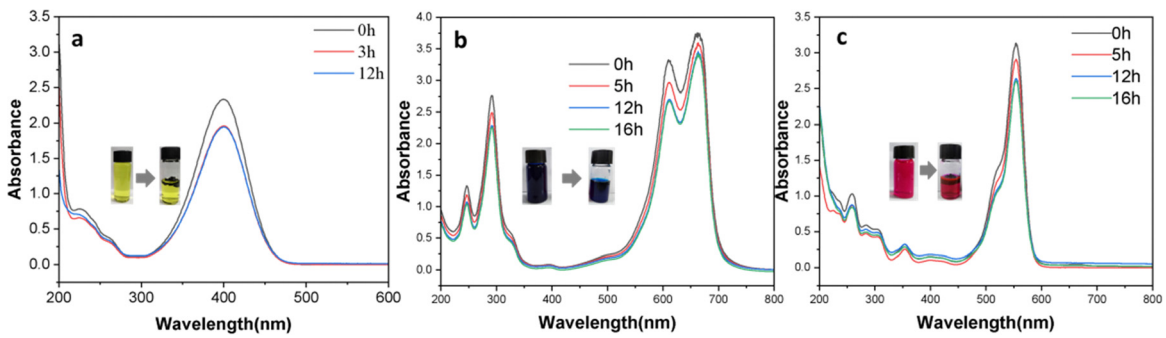

Fig. 6 (a) UV-VIS spectra of 4-NP adsorbed by GA–Fe_3O_4–Au–$_{ethanol}$. (b) UV-VIS spectra of methylene blue adsorbed by GA–Fe_3O_4–Au–$_{ethanol}$. (c) UV-VIS spectra of rhodamine adsorbed by GA–Fe_3O_4–Au–$_{ethanol}$.

the accumulation of flake particles, and does not exhibit adsorption saturation in the higher relative pressure region. One can infer from the aperture distribution that the material has commonly present pores smaller than 10 nm, which may be

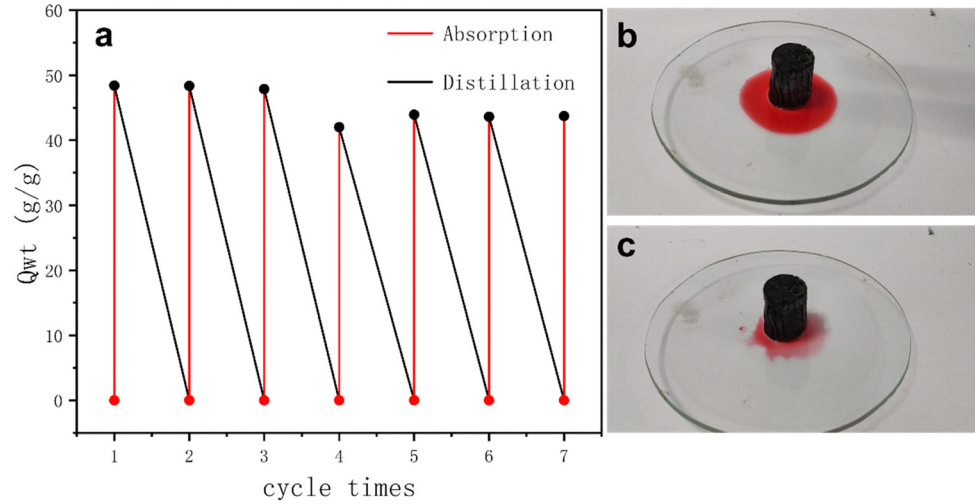

Fig. 7 (a) Cyclic adsorption of *n*-dodecane by materials (b and c) Schematic diagram of dodecane dyed with oil red adsorbed by materials.

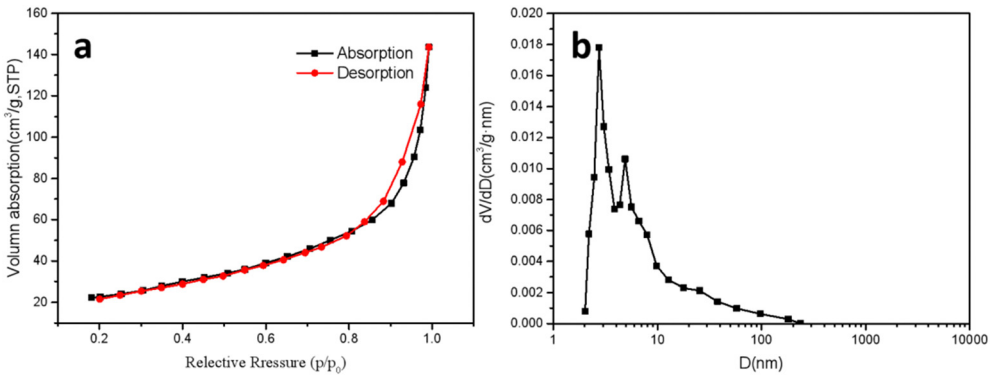

Fig. 8 (a) Isothermal nitrogen adsorption and desorption curve of GA–Fe_3O_4–Au–$_{ethanol}$. (b) Aperture distribution curve of GA–Fe_3O_4–Au–$_{ethanol}$.

attributed to the release and extrusion of nanoparticles from graphene layers during preparation.

4. Conclusion

By utilizing radiation reduction technology, the Au nanoparticles were successfully combined with reduced graphene oxide and ferroferric oxide was introduced into the composite. GA–Fe_3O_4–Au–$_{ethanol}$ composites that magnets can attract are synthesized effectively and simply using a one-step method. It is found that the composite can be used as a catalyst to degrade the pollutant 4-NP effectively. Its catalytic performance is linear with the concentration of AuNPs in the composite, and the catalysis follows the pseudo-first-order kinetics. At the same time, the adsorption capacity of the composite for organic dye solution is also explored. It is found that the composite has a specific adsorption capacity for organic dye solution.

Conflicts of interest

There is no conflict of interest to declare.

Acknowledgements

This work was supported financially by the Gansu Natural Science Foundation (Project no. 20JR10RA778 and 20JR10RA777).

References

1 M. Teimouri, F. Khosravi-Nejad, F. Attar, A. A. Saboury, I. Kostova, G. Benelli and M. Falahati, Gold nanoparticles fabrication by plant extracts: synthesis, characterization, degradation of 4-nitrophenol from industrial wastewater, and insecticidal activity – A review, *J. Cleaner Prod.*, 2018, **184**, 740–753, DOI: 10.1016/j.jclepro.2018.02.268.

2 B. L. Cushing, V. L. Kolesnichenko and C. J. O'Connor, Recent advances in the liquid-phase syntheses of inorganic nanoparticles, *Chem. Rev.*, 2004, **104**(9), 3893–3946, DOI: 10.1021/cr030027b.

3 K. D. N. Vo, C. Kowandy, L. Dupont, X. Coqueret and N. Q. Hien, Radiation synthesis of chitosan stabilized gold nanoparticles comparison between e(-) beam and gamma irradiation, *Radiat. Phys. Chem.*, 2014, **94**, 84–87, DOI: 10.1016/j.radphyschem.2013.04.015.

4 J. Huang, X. Z. Li, R. H. Xie, X. L. Tan, J. B. Xi, F. Tian, P. Liu, T. W. Hansen and Z. W. Bai, Defect anchoring of atomically dispersed Pd on nitrogen-doped holey carbon nanotube for catalytic hydrogenation of nitroarenes, *Appl. Surf. Sci.*, 2023, **615**, 156344, DOI: 10.1016/j.apsusc.2023.156344.

5 D. Wang, Y. Li, L. S. Wen, J. B. Xi, P. Liu, T. W. Hansen and P. Li, Ni-Pd-Incorporated Fe3O4 Yolk-Shelled Nanospheres as Efficient Magnetically Recyclable Catalysts for Reduction of N-Containing Unsaturated Compounds, *Catalysts*, 2023, **13**(1), 190, DOI: 10.3390/catal13010190.

6 L. S. Wen, D. Wang, J. B. Xi, F. Tian, P. Liu and Z. W. Bai, Heterometal modified Fe3O4 hollow nanospheres as efficient catalysts for organic transformations, *J. Catal.*, 2022, **413**, 779–785, DOI: 10.1016/j.jcat.2022.07.036.

7 N. Zhang, Y. Qiu, H. Y. Sun, J. F. Hao, J. Chen, J. B. Xi, J. Liu, B. J. He and Z. W. Bai, Substrate-Assisted Encapsulation of Pd-Fe Bimetal Nanoparticles on Functionalized Silica Nanotubes for Catalytic Hydrogenation of Nitroarenes and Azo Dyes, *ACS Appl. Nano Mater.*, 2021, **4**(6), 5854–5863, DOI: 10.1021/acsanm.1c00777.

8 J. B. Xi, H. Y. Sung, D. Wang, Z. Y. Zhang, X. M. Duan, J. W. Xiao, F. Xiao, L. M. Liu and S. Wang, Confined-interface-directed synthesis of Palladium single-atom catalysts on graphene/amorphous carbon, *Appl. Catal., B*, 2018, **225**, 291–297, DOI: 10.1016/j.apcatb.2017.11.057.

9 J. A. Herrera-Melian, A. J. Martin-Rodriguez, A. Ortega-Mendez, J. Arana, J. M. Dona-Rodriguez and J. Perez-Pena, Degradation and detoxification of 4-nitrophenol by advanced oxidation technologies and bench-scale constructed wetlands, *J. Environ. Manage.*, 2012, **105**, 53–60, DOI: 10.1016/j.jenvman.2012.03.044.

10 Z. Zhang, G. Sebe, X. S. Wang and K. C. Tam, Gold nanoparticles stabilized by poly(4-vinylpyridine) grafted cellulose nanocrystals as efficient and recyclable catalysts, *Carbohydr. Polym.*, 2018, **182**, 61–68, DOI: 10.1016/j.carbpol.2017.10.094.

11 M. Arif, M. Shahid, A. Irfan, J. Nisar, W. T. Wu, Z. H. Farooqi and R. Begum, Polymer microgels for the stabilization of gold nanoparticles and their application in the catalytic reduction of nitroarenes in aqueous media, *RSC Adv.*, 2022, **12**(9), 5105–5117, DOI: 10.1039/d1ra09380k.

12 F. Saira, N. Firdous, R. Qureshi and A. Ihsan, Preparation and catalytic evaluation of Au/gamma-Al2O3 nanoparticles for the conversion of 4-nitrophenol to 4-aminophenol by spectrophotometric method, *Turk. J. Chem.*, 2020, **44**(2), 448–460, DOI: 10.3906/kim-1910-21.

13 Y. H. Zhang, F. Gao and M. L. Fu, Composite of Au-Pd nanoalloys/reduced graphene oxide toward catalytic selective organic transformation to fine chemicals, *Chem. Phys. Lett.*, 2018, **691**, 61–67, DOI: 10.1016/j.cplett.2017.10.060.

14 X. X. Yu, Y. J. Dai, Y. R. Wu, Y. F. Cheng and Q. S. Zhao, Synthesis of a Novel Magnetically Retrievable Nanocomposite with Au Nanocatalysts for Hydration Reaction, *Catalysts*, 2019, **9**(10), 789, DOI: 10.3390/catal9100789.

15 J. Li, J. Li, H. Meng, S. Xie, B. Zhang, L. Li, H. Ma, J. Zhang and M. Yu, Ultra-light, compressible and fire-resistant graphene aerogel as a highly efficient and recyclable absorbent for organic liquids, *J. Mater. Chem. A*, 2014, **2**(9), 2934–2941, DOI: 10.1039/c3ta14725h.

16 Y. L. He, J. H. Li, L. F. Li and J. Y. Li, Gamma-ray irradiation-induced reduction and self-assembly of graphene oxide into three-dimensional graphene aerogel, *Mater. Lett.*, 2016, **177**, 76–79, DOI: 10.1016/j.matlet.2016.04.187.

17 X. Y. Zhu, G. D. Zhu, Y. X. Ge, B. S. Zhang, J. M. Yang, B. Hu and J. Y. Liu, AU(nano)/Fe-MOF hybrid electrode for highly sensitive determination of trace As(III), *J. Electroanal. Chem.*, 2021, **899**, 115642, DOI: 10.1016/j.jelechem.2021.115642.

18 Y. Xu, G. Wang, L. J. Zhu, W. S. Deng, C. T. Wang, T. H. Ren, B. K. Zhu and Z. X. Zeng, Desert beetle-like microstructures bridged by magnetic Fe(3)O4 grains for enhancing oil-in-water emulsion separation performance and solar-assisted recyclability of graphene oxide, *Chem. Eng. J.*, 2022, **427**, 130904, DOI: 10.1016/j.cej.2021.130904.

19 J. Fan, Z. Shi, M. Lian, H. Li and J. Yin, Mechanically strong graphene oxide/sodium alginate/polyacrylamide nanocomposite hydrogel with improved dye adsorption capacity, *J. Mater. Chem. A*, 2013, **1**(25), 7433–7443, DOI: 10.1039/c3ta10639j.

20 L. Zang, L. Sun, S. Zhang, C. Finnerty, A. Kim, J. Ma and B. Mi, Nanofibrous hydrogel-reduced graphene oxide membranes for effective solar-driven interfacial evaporation and desalination, *Chem. Eng. J.*, 2021, **422**, 129998, DOI: 10.1016/j.cej.2021.129998.

21 S. H. Lee, H. J. Jung, S. J. Lee, J. Theerthagiri, T. H. Kim and M. Y. Choi, Selective synthesis of Au and graphitic carbon-encapsulated Au (Au@GC) nanoparticles by pulsed laser ablation in solvents: Catalytic Au and acid-resistant Au@GC nanoparticles, *Appl. Surf. Sci.*, 2020, **506**, 145006, DOI: 10.1016/j.apsusc.2019.145006.

22 S. Xuan, Y.-X. J. Wang, J. C. Yu and K. C.-F. Leung, Preparation, Characterization, and Catalytic Activity of Core/Shell Fe3O4@Polyaniline@Au Nanocomposites, *Langmuir*, 2009, **25**(19), 11835–11843, DOI: 10.1021/la901462t.

23 L. L. Xiong, R. Huang, H. H. Chai, L. Yu and C. M. Li, Facile Synthesis of Fe3O4@Tannic Acid@Au Nanocomposites as a Catalyst for 4-Nitrophenol and Methylene Blue Removal, *ACS Omega*, 2020, **5**(33), 20903–20911, DOI: 10.1021/acsomega.0c02347.

24 R. F. Zhang, P. W. Zheng and X. F. Ma, Preparation and catalytic properties of magnetic rectorite-chitosan-Au composites, *J. Alloys Compd.*, 2017, **690**, 381–389, DOI: 10.1016/j.jallcom.2016.08.131.

25 K. Fan, D. Li, L. Li, J. Li and F. Xu, Preparation of Fe3O4-doped magnetic graphene aerogels via radiation method in ethanol-H2O solution, *Fullerenes, Nanotubes, Carbon Nanostruct.*, 2022, **30**(12), 1207–1211, DOI: 10.1080/1536383x.2022.2084081.

